ITO/Au/ITO Sandwich Structure for Near-Infrared Plasmonics

Xu Fang,[†] Chee Leung Mak,[‡] Jiyan Dai,[‡] Kan Li,[†] Hui Ye,*,[†] and Chi Wah Leung*,[‡]

[†]State Key Laboratory of Modern Optical Instrumentation, Department of Optical Engineering, Zhejiang University, Hangzhou, 310027, P. R. China

[‡]Department of Applied Physics, The Hong Kong Polytechnic University, Hung Hom, Hong Kong, P. R. China

Ⓢ *Supporting Information*

ABSTRACT: ITO/Au/ITO trilayers with varying gold spacer layer thicknesses were deposited on glass substrates by pulsed laser deposition. Transmission electron microscopy measurements demonstrated the continuous nature of the Au layer down to 2.4 nm. XRD patterns clearly showed an enhanced crystallinity of the ITO films promoted by the insertion of the gold layer. Compared with a single layer of ITO with a carrier concentration of 7.12×10^{20} cm^{-3}, the ITO/Au/ITO structure achieved an effective carrier concentration as high as 3.26×10^{22} cm^{-3}. Transmittance and ellipsometry measurements showed that the optical properties of ITO/Au/ITO films were greatly influenced by the thickness of the inserted gold layer. The cross-point wavelength of the trilayer samples was reduced with increasing gold layer thickness. Importantly, the trilayer structure exhibited a reduced loss (compared with plain Au) in the near-infrared region, suggesting its potential for plasmonic applications in the near-infrared range.

KEYWORDS: *transparent conductive oxide, ITO/Au/ITO, pulsed laser deposition, electrical and optical properties, plasma frequency*
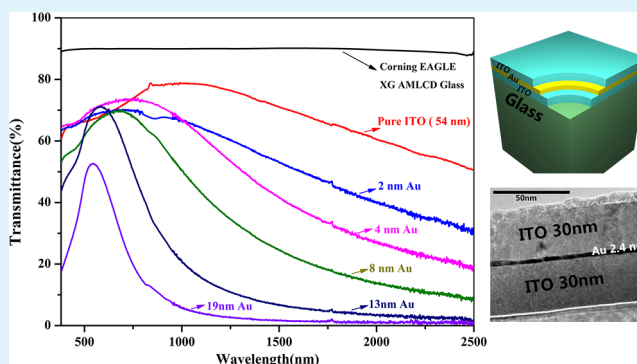
■ INTRODUCTION

Noble metals such as gold and silver have been predominantly used in the field of nanophotonics,[1] plasmonics,[1,2] and metamaterial[3,4] devices because of their high carrier concentration N ($N_{Au} = 5.90 \times 10^{22}$ cm^{-3}, $N_{Ag} = 1.07 \times 10^{22}$ cm^{-3}) and low resistivity values. However, such metals are not optimal for plasmonic devices operating in the near-infrared (NIR) range because of the large optical losses and high negative real-part permittivities.[5] Recently, because of the unique plasmon dispersion relationship, plasmonics with two-dimentional materials (e.g., graphene[6,7]) or nanosized materials (e.g., nanoflakes of MoO_3[8]) have attracted lots of attention. Unfortunately, the plasmons in these materials were all observed in the mid-IR or longer wavelengths because of the insufficient carrier densities.

Transparent conductive oxides (TCOs, such as Sn-doped In_2O_3 (ITO), Ga-doped ZnO (GZO), and Al-doped ZnO (AZO)) are promising materials for NIR plasmonics because of their low losses in the NIR region.[5,9−13] Advantages of TCOs over noble metals include tunable optical properties according to the deposition conditions and doping concentration, as well as their chemical and mechanical stabilities.[10] Various potential applications in plasmonics such as sensing,[14,15] localized surface plasmon resonances (LSPR),[16,17] photovoltaic and photocatalytic,[18] and optofluidic applications[19] based on TCOs have been explored.

On the other hand, their relatively low carrier concentrations (10^{20}–10^{21} cm^{-3} even at ultrahigh doping levels) result in

crossover wavelengths (at which a sign change for the real-part of permittivity occurs) around 1500 nm or longer.[11−13,20−24] At shorter wavelengths, surface plasmon is hardly or weakly excited between the ITO and the dielectric interfaces. Unfortunately, because of the low solid-solubility limits of dopants and low ionization efficiencies, further improvement of TCO carrier concentration faces significant challenges.[11]

Recently, semiconductor/noble metal/semiconductor structures were investigated with the aim of improving the electrical and optical properties of TCOs.[25] In such a structure, the noble metal is invariably Ag or Au, and the semiconductors used include ITO,[26−31] ZnO,[32,33] and AZO.[34−37] For example, Sytchkova et al.[38] and Guske et al.[39] systematically investigated the optical and plasmonic properties of sputtered AZO/Ag/AZO sandwich structures by varying the thickness of the silver spacer. However, the problem encountered in both studies was that the inserted metal spacer became discontinuous or porous when the magnetron-sputtered Ag layer thickness was less than a critical value (~10 nm). As a consequence, detrimental effects (optical scattering, electron scattering) induced by the metal spacer should be considered when performing optical and electrical characterization. A structure consisting of flat, continuous, and ultrathin (less than 10 nm) metal insertion layer sandwiched by TCO layers remains to be investigated.

In this paper, we report the growth of ITO/Au/ITO sandwich structures and performed electrical and optical characterizations from the visible range to NIR. As compared with doped ZnO (AZO[40] or GZO[41]), ITO exhibits relatively high carrier concentration if deposited at right temperatures.[42] Besides, doped ZnO (AZO or GZO) shows less electrical stability than ITO with thickness less than 30 nm.[43] ITO was therefore chosen as the TCO material.

Pulsed laser deposition (PLD) was employed to fabricate the samples without breaking the vacuum. ITO/Au/ITO trilayers with continuous Au insertion layer (thickness down to 2.4 nm) were successfully prepared and confirmed by transmission electron microscopy (TEM). The optical properties of the trilayer structure with different Au thicknesses were investigated by optical transmittance and spectroscopic ellipsometry measurements. The crossover wavelength of the composite structure's real-part permittivity was found shifting to shorter wavelengths as the thickness of the gold layer increased. Such a structure offers the potential in plasmonic devices (sensors, plasmonic waveguide, etc.) that operate in the NIR region.

■ EXPERIMENT DETAILS

ITO/Au/ITO trilayers were deposited in a PLD system equipped with a KrF excimer laser source (Coherent, Compex Pro 205 F, λ = 248 nm, pulse duration of 25 ns) without breaking the vacuum.[44] During the deposition, 300 mJ laser pulses at a repetition of 5 Hz were focused on the surfaces of the targets. The ITO target used in this work was a 10 wt % SnO_2-doped In_2O_3 disk (purity 99.99%). Gold target of purity 99.99% was used for the deposition of the insertion layer.

All the films were grown on Corning glass substrates (Corning Eagle XG AMLCD glass) with an area of 10 mm × 10 mm and thickness of 0.7 mm. The glass substrates were ultrasonically cleaned in acetone, ethanol and deionized water for 20 min and were subsequently dried with a flow of nitrogen. The substrates were attached to the substrate holder in the PLD system with silver conductive paint. The chamber base pressure was better than 2×10^{-3} mTorr. The substrates were heated to 100 °C during the film deposition process because ITO films deposited at room temperature tend to show high resistivity (10^{-1} $\Omega \cdot$cm), while higher temperatures cause Au layer clustering.[45] The specific conditions of depositing the ITO and Au layers are listed in Table 1. During the film deposition process, the targets were kept rotating to avoid localized damages.

Table 1. Deposition Parameters of ITO and Gold Layers

	ITO	Au
base pressure (mTorr)	2×10^{-3}	2×10^{-3}
repetition frequency (Hz)	5	5
laser fluence (mJ·cm^{-2})	0.15	0.12
O_2 pressure (mTorr)	1	vacuum
target to substrate distance (mm)	40	50
substrate temperature (°C)	100	100
layer thickness (nm)	30	2.4−19

The microstructure and crystallinity of the films were inspected by X-ray diffractometry (XRD, Rigaku Smart Lab with Cu Kα, λ = 1.5406 nm). The surface morphologies of the films were analyzed using field emission scanning electron microscopy (FE-SEM, JEOL model JEM-6335F), and the surface roughness was measured over 10 μm × 10 μm of sample surfaces by atomic force microscopy (AFM, Xe-100, Park System Corporation) under ambient conditions. To investigate the electrical properties (carrier concentration, resistivity, and Hall mobility) of the samples, four-point probes measurements (Ecopia, HMS-5000) were performed with the van der Pauw configuration.[46] Direct transmittances of the samples were obtained with Shimadzu UV-3101 spectrophotometer in the range of 400−2500 nm. Bare glass

substrates used in this work exhibited 91% transmittance within this range. Ellipsometric investigations were performed with a GES-5E instrument (Semilab) in the range of 600−2000 nm. The optical permittivities of the samples were obtained by fitting the ellipsometric angles ψ and Δ using the WinElli II software.

■ RESULTS AND DISCUSSION

The XRD measurement results are presented in Figure 1. When the gold spacer is absent, no peak can be observed, meaning
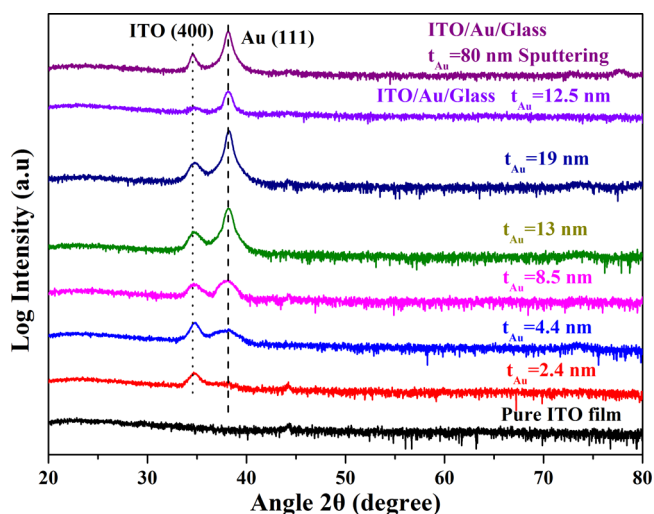

Figure 1. XRD pattern of ITO single layer and ITO/Au/ITO trilayer films with different gold insertion layer thicknesses. Also shown are the spectra of ITO (30 nm)/Au bilayers of two different Au thicknesses (see labels for details). The positions for ITO (400) and Au (111) peaks are indicated as dotted and dashed lines in the figure, respectively. Spectra for different samples are offset for clarity.

that pure ITO films deposited under the conditions of Table 1 are amorphous. After insertion of the gold layer, an indium oxide (400) peak is revealed even with 2.4 nm of Au insertion layer. All the XRD spectra of the trilayer samples exhibit two peaks at (34.7° ± 0.1°) and (38.2° ± 0.1°), which correspond to the bixbyite structure indium oxide (400) and Au (111), respectively.[29,30] As expected, the Au (111) peak becomes sharper and stronger with thicker gold spacers. By comparison with the standard XRD patterns of indium oxide (In_2O_3 PDF no. 06-0416), tin oxide (SnO PDF no. 06-0395, SnO_2 PDF no. 41-1445), and gold (PDF no. 04-0784), the possible phases near the small peak (44.3° ± 0.1°) are SnO_2 (210) at 42.634°, SnO (102) at 44.392°, In_2O_3 (422) at 43.781°, and Au (200) at 44.392°. As this small peak also appears in the plain ITO pattern, it should correspond to the phase of SnO (102).

To further explore whether the inserted gold layer was able to improve the crystallinity of the upper ITO layer, ITO films with Au buffers were also prepared on glass substrates and characterized (hereafter ITO/Au bilayers for brevity). The spectra of ITO/Au bilayers with different gold buffer layer thicknesses (12.5 and 80 nm) are shown at the top of Figure 1. Both the bilayer samples exhibit the same indium oxide (400) and Au (111) peaks as the trilayer samples. Given the absence of crystallinity in the bottom ITO layer (as evidenced from the pure ITO film spectrum), we attribute the improved ITO crystallinity to that of the upper ITO layer. We should also notice that while there seems to be a strong dependence of ITO crystallinity on the Au thickness in bilayer samples, a high level of crystallinity can be obtained in the trilayers even with 2.4 nm

of Au spacer. As reported,[47] ITO films deposited below 150 °C are generally amorphous, irrespective of the technique used. Thus, we can infer that the inserted Au layer has improved the crystallinity of the ITO films by acting as a crystalline substrate. The improvement of crystallinity is attributed to the Au's continuous nature (as shown in TEM measurement in Figure 2) with (111) orientation, which acts as a substrate for the
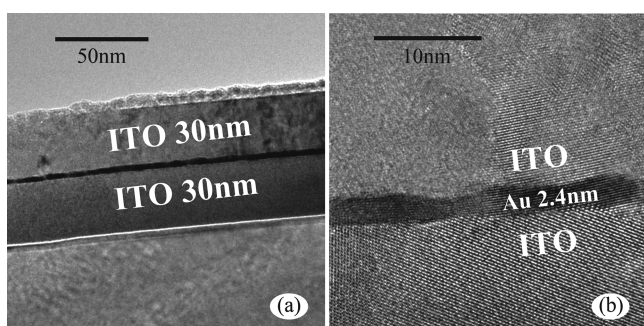

Figure 2. (a) TEM cross-section micrographs of the ITO (30 nm)/Au (2.4 nm)/ITO (30 nm) sample. Enlarged HRTEM image (b) shows the thickness uniformity of the gold spacer.

subsequently crystalline growth of the upper ITO layer.[29] It was also reported in literature that Ni buffers could induce crystallization of the otherwise amorphous silicon thin films as a result of $NiSi_2$ formation at the interface;[48] judging from the sharp ITO/Au interfaces in the TEM micrographs, however, we eliminate the possibility of any compound formation in our samples.

TEM was employed to obtain the film thickness and inspect the homogeneity of the layers in the sandwich structure. The TEM micrographs in Figure 2 show the trilayer sample with the thinnest Au spacer (2.4 nm) at different magnifications. The Au

spacer shows good uniformity across the sample. Typically Au deposited directly on glass substrates forms nanoclusters due the low surface energy, and a substrate treatment is often needed to improve the homogeneity of Au deposited on glass surfaces.[49] The introduction of ITO buffer layer greatly improves the wetting conditions of gold,[50,51] transforming the gold film from island-like growth to layered growth at lower thickness. This also echoes with the improved crystallinity of the upper ITO layer in the trilayer samples with ultrathin Au spacer: the uniform Au coverage on ITO bottom layer ensures the growth of crystalline ITO upper layer, as contrasted with the island-like Au grains that form on quartz and ITO surface.[45,52] It was reported[53] that continuous ITO film of 2.5 nm could be deposited by PLD on glass substrates at 100 °C (which is the temperature of deposition in this work). It would be of interest to explore the optical and electrical properties of ITO/Au/ITO sandwiches as the layer thickness approaches the limit for continuous film growth.

Figure 3 illustrates the evolution of surface morphology during the growth of the trilayers by investigating the build-up samples of the trilayer structure with AFM.[54] As can be seen from Figure 3a, the 30 nm bottom ITO layer deposited on glass has a relatively large surface roughness (root-mean-squared roughness σ_{rms} = 0.61 nm). The deposition of 8.5 nm thick gold on ITO (Figure 3b) results in a reduced σ_{rms} of 0.47 nm. Finally, for the complete trilayer (Figure 3c) with 30 nm of ITO on the Au surface, it has a σ_{rms} of 0.44 nm. The decrease of σ_{rms} can be explained by the improved wetting condition on the surface of the bottom ITO film. At first an amorphous ITO layer is deposited on the glass substrate, followed by the smooth and flat Au spacer layer with (111) orientation, which induces the crystalline growth of the upper ITO film with an improved surface morphology. The ability of PLD technique in producing high-quality films could also contribute to the low σ_{rms} of the top ITO, as the typical initial velocity of the atoms
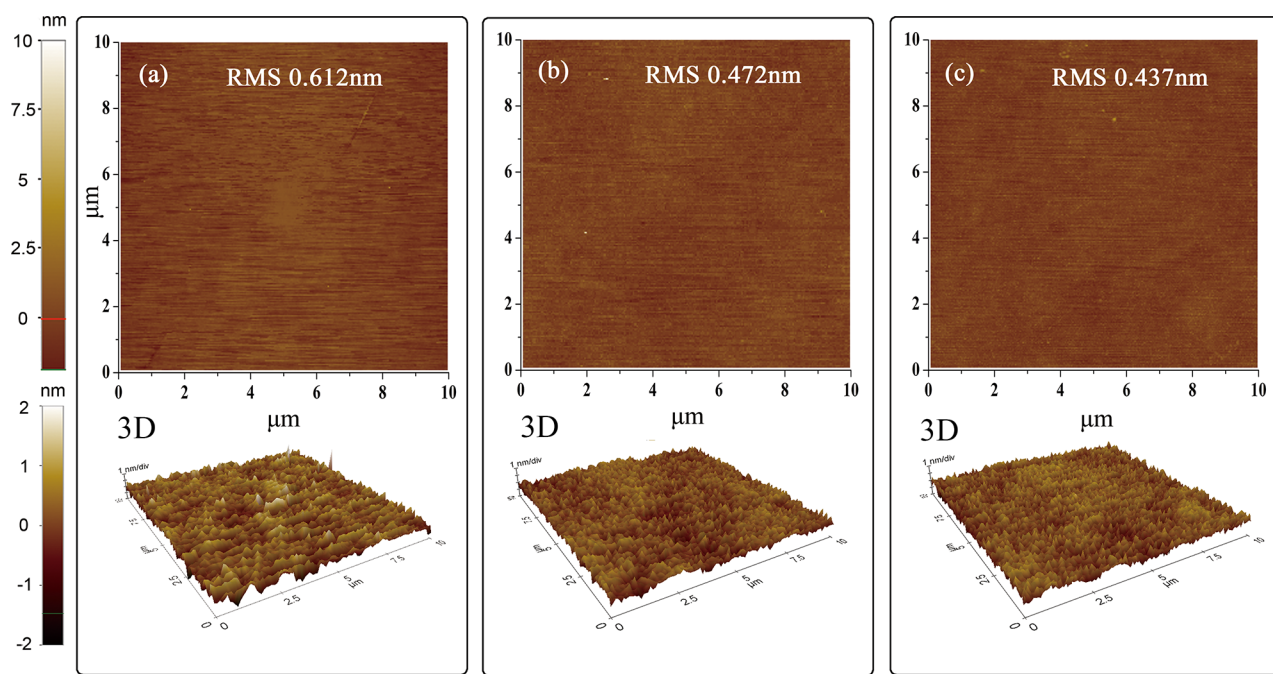

Figure 3. Evolution of surface morphology (planar and 3D mode) in ITO (30 nm)/Au (8.5 nm)/ITO (30 nm) by AFM of build-up samples: (a) 30 nm ITO layer (σ_{rms} = 0.612 nm); (b) 8.4 nm Au on 30 nm ITO (σ_{rms} = 0.472 nm); (c) ITO (30 nm)/Au (8.4 nm)/ITO (30 nm) (σ_{rms} = 0.437 nm). Scan area is 10 μm × 10 μm for all scans.

or ions is $\geq 10^4$ m·s^{-1} (kinetic energy of $\geq$52 eV) in the ablation plume.[55] Such excitation energies of ablated species efficiently increase the nucleation density on the surface as compared to traditional sputtering or thermal evaporation methods.[55] Thus, the increased nucleation density results in an improved smoothness of the deposited films.

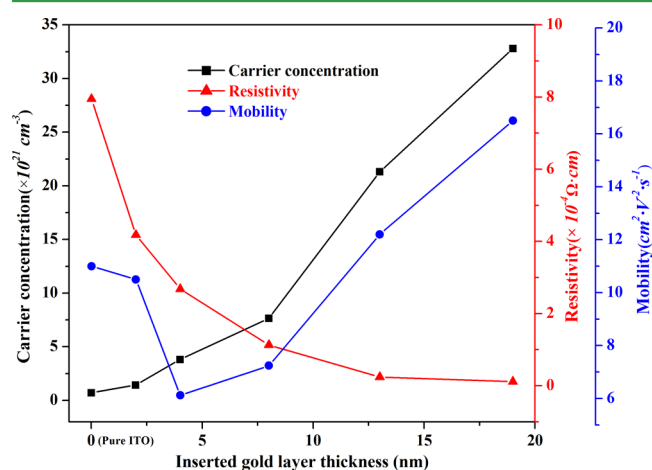Figure 4 presents the electrical properties (carrier concentration N (■), resistivity ρ (▲), and Hall mobility μ (●)) of

Figure 4. Carrier concentration ($\times 10^{20}$ cm^{-3}), resistivity ($\times 10^{-4}$ Ω·cm), and Hall mobility (cm^2·V^{-1}·s^{-1}) of trilayers as a function of the inserted gold layer thickness.

the samples. The plain ITO film owns the lowest N (7.12×10^{20} cm^{-3}) and the highest ρ (7.95×10^{-4} Ω·cm) among all the samples. After addition of the Au insertion layer, the carrier concentration of the trilayer samples rapidly and monotonically increases up to 3.28×10^{22} cm^{-3} as the Au thickness rises from 2.4 to 19 nm. At the same time the insertion of the Au spacer leads a significant reduction of ρ from 4.18×10^{-4} to 1.15×10^{-5} Ω·cm. Such a monotonous variation with Au spacer thickness does not happen to the Hall mobility. Pure ITO film has a relatively high mobility of 11 cm^2·V^{-1}·s^{-1}, which drops to a minimum for the trilayer with 4.4 nm of gold spacer. In general, carrier density and mobility of the ITO films are influenced by the oxygen vacancies and concentration of

substituted Sn^{4+} on In^{3+} sites.[56] In this study all the ITO films were prepared under identical conditions, so the oxygen vacancies and doping should not lead to an increased carrier concentration. It was suggested[30] that the increase of N in ITO/Au/ITO layers is due to the larger grain size (small grain boundary density), which is accompanied by the decrease of ρ. Also because of the insertion of the Au spacer, the crystallinity of the upper ITO film has shown an improvement, which in turn reduces the grain boundary density within the upper ITO film (which was also observed in the ellipsometry data as discussed later). Thus, the improved crystallinity of the upper ITO layer would result in an improvement on the μ. The presence of a minimum in μ can be understood as the competing effects of bulk conduction (which allows high-mobility transport) and interfacial scattering (which suppresses the mobility values). With the absence the Au layer μ is solely determined by the bulk of ITO. The insertion of Au introduces two Au/ITO interfaces, which severely affects the electron transport and lowers μ. Eventually the increasing Au thickness permits electron transport across the bulk of Au (which has a low resistivity) and leads to a revival of μ in the whole sample.

The spectral transmittance (380–2500 nm) of trilayer samples as a function of Au insertion layer thickness is illustrated in Figure 5a. The transmittance of glass substrate (>90%) and plain ITO layer (nominally identical to the trilayer structure with zero Au spacer thickness) are also displayed for comparison. It is obvious that the overall transmittance of the trilayer structure is highly influenced by the thickness of the inserted gold layer. For a single ITO film the highest transmittance is 79% at 990 nm, which decays to about 50% at 2500 nm. The trilayer with 2.4 nm of gold spacer has a relatively low transmittance in the visible range due to the absorption and scattering by the gold spacer. It can be noted that trilayer samples with 2.4–8.5 nm thick gold spacers show higher transparencies than single ITO films between 450 and 650 nm; this is due to the interference effect introduced by the inserted gold films.[56−58] In order to further explain such an antireflectance phenomenon, a simulated direct transmittance based on the transfer matrix theory is presented in Figure 5b. The simulation results indicate the changes of transmittance with different thicknesses of the inserted gold spacer, which are identical to those observed from the measured transmittance.
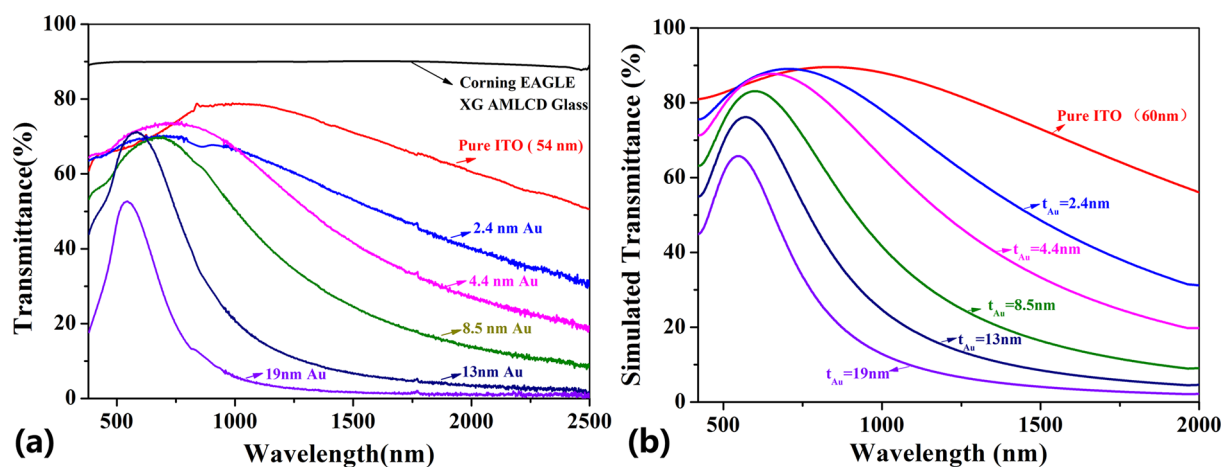

Figure 5. (a) Direct spectral transmittance of trilayer samples with different gold spacer thicknesses. The transmittance of bare Corning glass substrate and a plain 54 nm ITO layer is illustrated for comparison. (b) Simulation of direct transmittance of ITO/Au/ITO trilayer structure as a function of Au spacer thickness based on the transfer matrix theory.
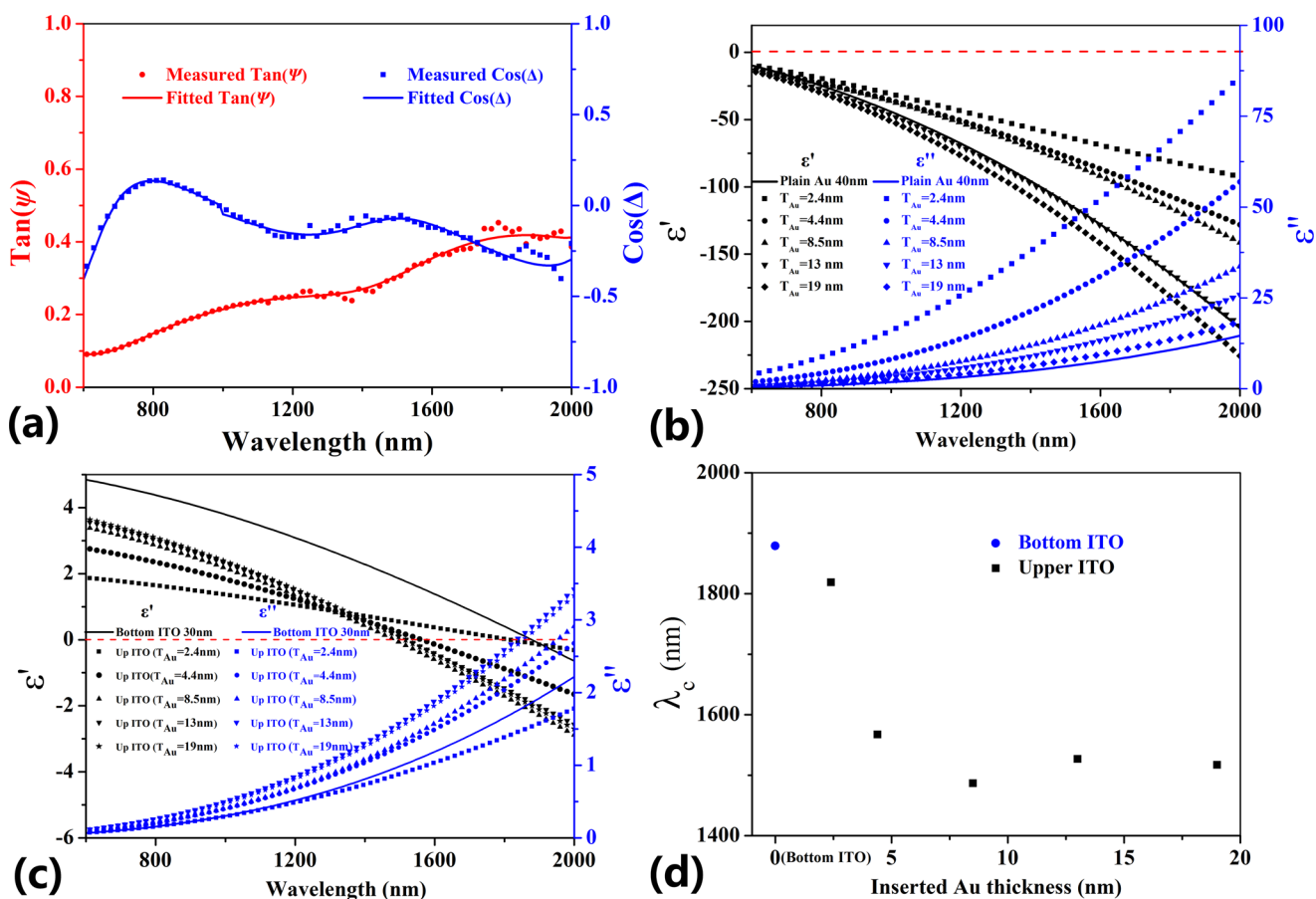
Figure 6. (a) Ellipsometric parameters, tan Ψ (red) and cos Δ (blue) for the trilayer sample with the thinnest Au spacer layer (2.4 nm). Points and lines correspond to the experimentally measured and model-fitted values, respectively. (b) ε' (black symbols) and ε'' (blue symbols) of the inserted Au spacer as a function of its thickness in the trilayer structure. Solid lines represent the permittivity of 40 nm plain Au on glass. (c) ε' (black symbols) and ε'' (blue symbols) of the upper ITO layer in trilayers with different Au thickness. Solid lines represent bottom ITO layer's permittivity. (d) Crossover wavelength (λ_c) of the bottom and upper ITO layers' real part permittivity as a function the inserted Au layer thickness.

For thicker gold spacers, the measured transmittance between 450 and 650 nm range decreases and forms a narrow transmission peak.

In the near-UV range the transmittance decreases linearly with increasing gold spacer thickness. For single ITO film and trilayer structure with 2.4 nm of Au spacer the fundamental absorption edge[30] is hard to be located because of the extremely broad transmittance peak. As the gold layer thickness increases, the absorption edge becomes sharper with the absorption edge shifting to larger wavelengths. Such a shift in the near UV term is consistent with the results of Bender et al.[59] and Kim et al.[30] In the near-IR range, transmittance decreases linearly with increasing Au spacer thickness, with the transparent region shrinking and shifting to lower wavelength. This shift is mainly caused by the increase of the reflectance,[59] as induced by the increase of plasma resonance frequency (ω_p) of the free electron gas within the inserted gold layer (due to the increased thickness) and the upper ITO layer (due to improved crystallinity and proved in the ellipsometry results), respectively. Just as shown in Figure 4, the sample carrier concentration N increases with rising Au insertion layer thickness. Assuming a homogeneous material, a higher carrier concentration would result in a larger ω_p:

$$\omega_p = \frac{Ne^2}{\varepsilon_\infty m^*} \qquad (1)$$

Here N is the carrier concentration, e is the electronic charge, m^* is the effective mass of an electron, and ε_∞ is the high frequency permittivity.[60] Consequently, by insertion of gold layers of different thicknesses between the ITO, the effective plasma resonance frequency of the trilayers will be tuned accordingly.

In order to investigate the trilayer structures' plasmonic properties as a function of the inserted gold layer thickness, spectroscopic ellipsometry was used to characterize the films in the spectral range 600−2000 nm at the incident angle of 62°. The ellipsometry data were fitted to extract the optical permittivity of each layer in the trilayer samples. An effective medium approximation was then introduced to get the effective permittivity of the trilayers in order to evaluate their plasmonic properties. Because of the different crystallinity of the upper and bottom ITO films in the trilayer structure (the upper ITO is polycrystalline while the bottom ITO is amorphous, as confirmed by the XRD measurements), the upper and bottom ITO films were treated as two independent materials. The permittivity of the bottom ITO film was fixed during the fitting process (assumed to be equal to the permittivity of the 54 nm thick ITO film deposited under identical conditions) on glass, while the thickness was a free parameter. The model used to describe the optical properties of each layer is the Drude model without adding any Cauchy or Lorentz model components. It was reported that because of the interband transition for Au

and onset of the band gap in ITO, it is hard to perform a purely Drude fit to the permittivity at wavelengths shorter than 500 nm.[60] Therefore, the fitting procedures were conducted in the range of 600–2000 nm, where the Drude model is valid for both materials. The Drude model is defined as follows:

$$\varepsilon_r = \varepsilon_\infty - \frac{\left(\frac{w_p}{w}\right)^2}{1 + \left(\frac{\Gamma}{w}\right)^2} \tag{2}$$

$$\varepsilon_i = \frac{i\left(\frac{w_p}{w}\right)^2 \frac{\Gamma}{w}}{1 + \left(\frac{\Gamma}{w}\right)^2} \tag{3}$$

Here Γ is the relaxation frequency and ω is the frequency of free light. As a result, the free parameters (nine in total) that need to be calculated are d_{ITO1}, $\varepsilon_{\infty,ITO1}$, Γ_{ITO1}, $\omega_{p,ITO1}$ (upper ITO), d_{Au}, $\varepsilon_{\infty,Au}$, Γ_{Au}, $\omega_{p,Au}$ (inserted Au spacer), and d_{ITO2} (bottom ITO).

The results of the fitting were very good as can be seen from Figure 6a, which illustrates the fitting parameters of the ITO/Au (2.4 nm)/ITO sample as compared with the measured data. The mean-square error (MSE) and coefficient of determination (R^2) of the ellipsometric parameter fittings were used to evaluate the difference between the measured and fitted curves.[61] The high similarity between the fitting and the measured data (MSE = 2.96×10^{-3}, $R^2 = 0.91$) exhibited the reliability of the models and structures in retrieving the permittivity of each layer.

Figure 6b shows the variation of the inserted Au layer permittivity as a function of its thickness in the trilayer structure. For comparison, the permittivity of a 40 nm plain Au film on glass (fitted by ellipsometry measurement) is also shown. The evolution of the inserted Au layer's permittivity exhibits a strong dependence on its thickness. The 2.4 nm Au shows the smallest numerical value of $\varepsilon'_{Au,2.4nm}$ (−93) at 2000 nm, as compared to that of the plain Au $\varepsilon'_{Au,40nm}$ (−205) at 2000 nm; the 2.4 nm thick Au spacer also shows the largest imaginary part of permittivity ($\varepsilon''_{Au,2.4nm}$ = 86 at 2000 nm, approximately 6 times that of plain Au $\varepsilon''_{Au,40nm}$ = 15 at 2000 nm) among all the samples (comparison between the permittivity of 2.4 nm thick Au and bulk Au can be seen in Supporting Information Figure S1). The behavior of permittivity for the 2.4 nm thick Au is mainly caused by its lower carrier concentration and lower electron mobility as compared to the bulk Au, as a consequence of the small grain sizes (poor crystallinity of Au layer) which act like traps that decrease the carrier density and hinder the electronic transport. As the electron mobility is directly linked to the imaginary part of permittivity,[13,39] the lower mobility is responsible for the large ε'' of the 2.4 nm Au spacer. This low mobility was also confirmed by the Hall measurement: the mobility of the trilayer structure suffers a drop after the insertion of the 2.4 nm gold spacer (Figure 4). In addition to the mobility effect, the electron-surface scattering is another factor that is attributed to the large ε'' of 2.4 nm gold layer. For thin films or small particles[62−64] with thickness (dimensions) below the bulk electron mean free path (~37 nm at 300 K in Au),[63,64] the response of free-electrons can be greatly affected by electron surface scattering, resulting in enhanced plasmon damping (larger ε''). As the Au thickness increases, its properties get closer to that of the 40 nm plain gold film. The real-part

permittivity of 13 nm thick gold spacer is nearly the same as that of the plain Au film, while the imaginary part is slightly larger than that of the plain Au; such an observation suggests that the 13 nm Au film can effectively be treated as bulk. When the Au spacer is 19 nm in thickness, ε'' is very close to that of a plain Au film, but the numerical value of ε' is a little larger than that of the plain Au film. The strong dependence of the fitted Au layer's permittivity on the gold layer thickness provides references to researchers who are investigating the application of ultrathin continuous gold layers as plasmonic materials.

Figure 6c illustrates the evolution of upper ITO film's permittivity in different trilayer samples. The real and imaginary parts of the bottom ITO film's permittivity are represented as solid lines for comparison. It can be seen from the figure that the upper ITO film's property is highly dependent on the underlying Au film's thickness. The crossover wavelength (λ_c, the wavelength at which a sign change of ε' occurs) of the bottom and upper ITO films are shown in Figure 6d. The bottom ITO has a relatively large ε' (with $\lambda_c = 1879.2$ nm) and low ε'' as compared with the upper ITO in any trilayer sample prepared in this work; this coincides with the relatively low carrier concentration of the plain ITO film, which results from the amorphous crystallinity. On the contrary, the upper ITO in the trilayer structure is polycrystalline, and the crystallinity improves with increasing Au spacer thickness (Figure 1). When the inserted gold spacer is 2.4 nm, ε' of the upper ITO shows a sharp drop (compared with bottom ITO), with λ_c shortened to 1819 nm, and the ε'' is smaller than that of bottom ITO. This suppressed permittivity can be ascribed to the improvement of the crystallinity of the upper ITO film introduced by the inserted Au spacer, as good crystallinity helps to increase the grain size and reduce the density of grain boundaries that act as traps and reduces the carrier concentration. Also such grain boundaries hinder the transition of electrons, causing the low electron mobility that is closely linked to the large imaginary part of permittivity. As the gold layer becomes thicker to 8.5 nm, the permittivity of the upper ITO film increases, and λ_c shifts to a shorter wavelength. When the gold spacer thickness reaches 13 and 19 nm, the permittivity of upper ITO layer is stabilized with λ_c located around 1500 nm, meaning that the two upper ITO films possess identical optical and electrical properties. This similarity is mainly caused by the crystallinity improvement due to the inserted gold layer but with limitations: 13 nm of Au spacer is already thick enough to thoroughly improve the property of 30 nm upper ITO film. The different properties between the upper and bottom ITO layers provide evidence that the improved crystallinity has the ability of improving the optical and electrical properties of ITO film.

In order to evaluate the plasmonic properties of the trilayer structure, an effective medium approximation was introduced by treating the trilayer system as a single but optically anisotropic layer.[65] Such an effective medium approximation is widely used in literature to describe the effective permittivity of the superlattice structure, which is typically repeated bilayers.[12,65,66] As reported by Kim et al.,[67] any multilayered structure with repeating metal/dielectric subunits can be effectively considered as a single layer with hyperbolic dispersion. Korobkin et al.[68] evaluated the effective permittivity of SiO$_2$ (205 nm)/SiC (410 nm)/SiO$_2$ (205 nm) trilayer structure in the far-IR range (at which SiC is metallic) using such an approximation.[68] The components of the effective dielectric tensor parallel ($\varepsilon_\parallel$) and perpendicular ($\varepsilon_\perp$) to the
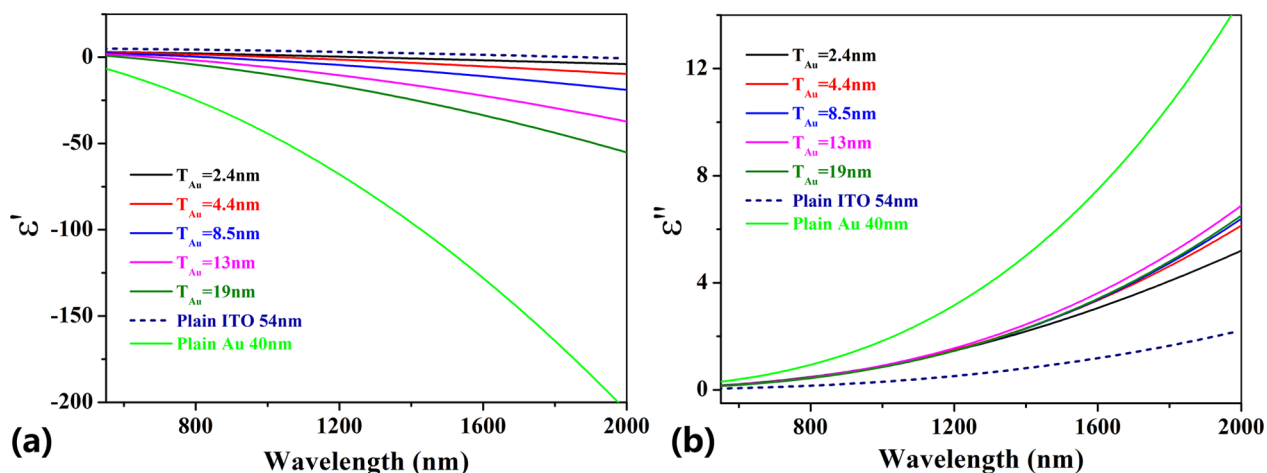
Figure 7. Real (ε') and imaginary (ε'') parts of effective $\varepsilon_\perp$ obtained using effective medium approximation.

anisotropy axis are given by (optical axis normal to the sample surface)

$$\varepsilon_\perp = \frac{1}{d_{ITO1} + d_{Au} + d_{ITO2}}(\varepsilon_{ITO1}d_{ITO1} + \varepsilon_{Au}d_{Au} + \varepsilon_{ITO2}d_{ITO2}) \quad (4)$$

$$\varepsilon_\parallel^{-1} = \frac{1}{d_{ITO1} + d_{Au} + d_{ITO2}}\left(\frac{d_{ITO1}}{\varepsilon_{ITO1}} + \frac{d_{Au}}{\varepsilon_{Au}} + \frac{d_{ITO2}}{\varepsilon_{ITO2}}\right) \quad (5)$$

It should be noted that surface plasmon polaritons are surface electromagnetic waves that propagate in a direction parallel to the conductive/dielectric interface. Besides, eq 4 is reliable only when each (optically isotropic) layer's thickness is much smaller than the wavelength (i.e., (d_{ITO1}, d_{Au}, d_{ITO2}) $\ll \lambda$); in our case such a requirement is definitely satisfied. Consequently, we take $\varepsilon_\perp$ as the parameter for evaluating the plasmonic property of the trilayer. In order to evaluate validity of the effective medium approximation, comparisons were made between the simulated transmittances of a trilayer structure and an effective layer. The transmittance of the effective layer at normal incidence is exactly the same as the trilayer (Figure S7a and Figure S3a of Supporting Information, respectively) and is comparable with the experimetal results (Figure 5a). For incident angle from 15° to 45°, the transmittances of s-polarized light (TE) on the effective layer is almost identical to that on the trilayer sample. As the incident angle increases to 60° and 75°, the differences between the two simulated structures become apparent. This gives evidence of the limitations of the effective medium approximation (large incident angle) in simulating the trilayer structure. Details of calculations and comparison can be seen in the Supporting Information Figures S2−S7.

Figures 7a and Figure 7b show the real and imaginary parts of the effective $\varepsilon_\perp$ of the trilayers. For comparison, the corresponding behavior of plain Au (40 nm) and ITO (54 nm) films on glass is also plotted. The plain ITO film has a positive ε' from the visible range to 1879 ± 5 nm, and acquires negative values at larger wavelengths; for gold ε' is always negative within the measured range and drops monotonically with increasing wavelength. Figure 7a shows a similar crossover of ε' to negative values for all the trilayers, as the wavelength increases from 600 to 2000 nm. It can be observed that λ_c is different among the trilayer samples. For direct comparison,

Figure 8 plots the variation of λ_c as a function of the Au spacer thickness. As λ_c is directly related to ω_p (which in turn is related

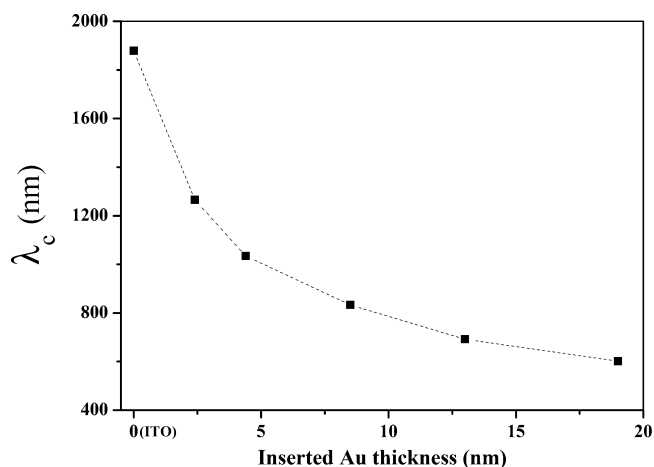**Figure 8.** λ_c of trilayer samples as a function of the gold spacer thickness.

to N), the phenomenon matches the Hall measurement results that N ascends with the rising Au spacer thickness. With the increase of N, there is a corresponding rise of ε'' that results in larger losses. Figure 7b clearly illustrates that plain ITO's ε'' is much smaller (≤ 2) than that of any trilayer sample or plain Au film. For the trilayers, ε'' rises with increasing Au spacer thickness except for the trilayer with the thickest (19 nm) Au spacer layer. This is due to the relatively improved ε'' of the 19 nm Au as obtained from ellipsometry measurements (Figure 6b). When compared with gold, all trilayers show lower losses within the measured wavelength range.

It would be of interest to evaluate the applicability of the ITO/Au/ITO structure in various applications.[13,69] To this end, we estimated the quality factor as applied in the fields of localized surface plasmon resonances (LSPR) and surface plasmon resonances (SPR). For LSPR the corresponding quality factor is defined as $Q_{LSPR(\omega)} = -\varepsilon_m'(\omega)/\varepsilon_m''(\omega)$, where $\varepsilon_m(\omega)$ is the permittivity of the plasmonic material. In the trilayer structure, $\varepsilon_m(\omega)$ represents the effective $\varepsilon_\perp$. For SPR, the quality factor is $Q_{SPP(\omega)} = \{[(\varepsilon_m'(\omega) + \varepsilon_d(\omega)]/[\varepsilon_m'(\omega)-\varepsilon_d(\omega)]\}\{(\varepsilon_m'(\omega)^2/\varepsilon_m''(\omega)\}$, where $\varepsilon_d(\omega)$ is the permittivity of the surrounding dielectric material, for which we choose SiO$_2$
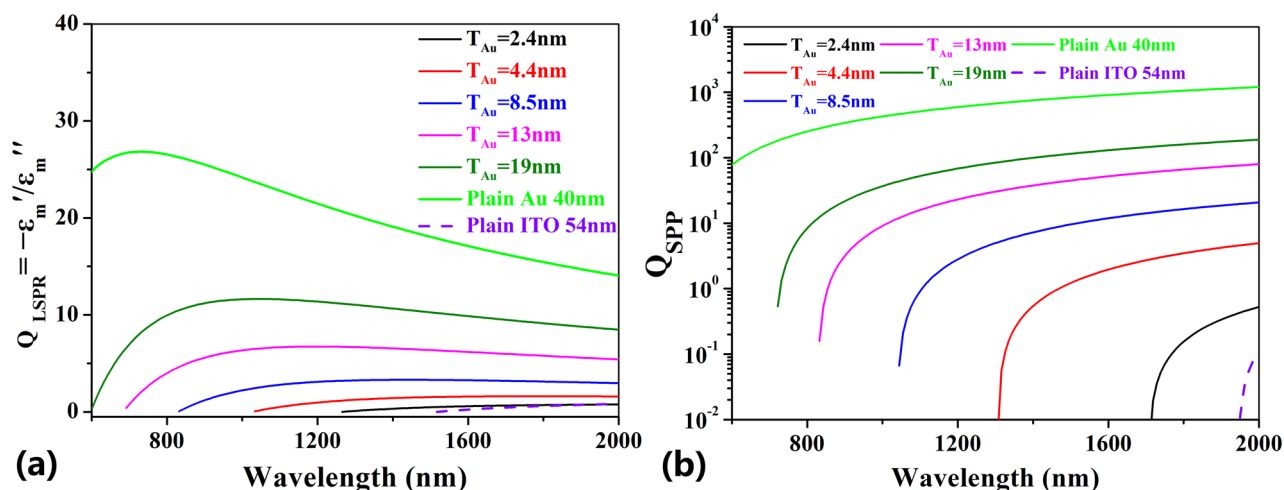
Figure 9. Quality factors of the trilayer samples for localized surface plasmon resonances (Q_{LSPR}, a) and surface plasmon polaritons (Q_{SPP}, b). The corresponding quality factors for plain Au and ITO films are also included for comparison.

(ε = 2.37 and is assumed constant in the calculated range (600−2000 nm)). $\varepsilon_m(\omega)$ is the permittivity of the plasmonic material. Here the data of Au are the permittivity of plain Au (40 nm) as extracted from the ellipsometry measurement. The permittivity of ITO is the fitted permittivity of the upper ITO on 19 nm Au spacer. The permittivity values for trilayer samples are the effective $\varepsilon_\perp$ of the trilayers with different Au spacer thicknesses.

Figure 9 shows the quality factors for the trilayer samples in LSPR and SPR modes. Plain Au surpasses the trilayer samples in these two applications, which is consistent with the reported data by Boltasseva et al.[13,69] On the other hand, all the trilayer samples have higher quality factors than plain ITO and show an increasing trend with rising Au spacer thickness.

We should stress that the quality factor cannot be the sole factor in judging the performance of such materials. The imaginary part permittivity for the trilayers with effective medium approximation $\varepsilon_\perp$ is small compared with Au; this property is important in applications such as transformation optics (TO). Also, as $\varepsilon_\perp$ is strongly related to the properties of the upper and bottom ITO films and the inserted Au spacer, this provides a means for manipulating the plasmonic behavior of the trilayer structure through the control of deposition conditions and Au spacer thicknesses. Furthermore, because of the weak chemical and mechanical stability of noble metals (even for gold), it is difficult to get reliable signals for long-time measurements.[70] The introduction of ITO upper layer not only improves the optical performance but also suppresses the degradation of the device.

Because of the relatively low carrier concentration of ITO films, the dielectric surrounding used to couple SPP resonance between ITO films is limited to low-permittivity materials such as air and SiO_2. By addition of an ultrathin gold layer between two ITO films, the effective permittivity of the hybrid structure is modulated according to the thickness of the Au spacer. This offers the potential application to excite SPP resonance between the ITO/Au/ITO hybrid film and Si ($\varepsilon \approx 11.9$ at 300 K) or Ge ($\varepsilon \approx 16$ at 300 K) surfaces at optical communication wavelengths. By introduction of an effective medium approximation, the plasmonic properties are evaluated. Through this method, not only we can couple SPP resonance between trilayer surface and dielectric surface at lower wavelengths (even in visible range) but also the imaginary

part of the trilayer structure can be kept smaller than pure gold, implying lower losses.

We caution that the validity of applying the equivalent permittivity for the ITO/Au/ITO structure depends on the thickness of individual layers. Issues such as distribution of SPP in the trilayer structure, as well as coupling of light into SPP in the trilayer from the surrounding, have to be addressed to justify the use of the equivalent permittivity model. Nevertheless, the present structure offers a simple and highly tunable means of adjusting the dielectric response of thin film structures in the NIR range, showing promise for plasmonic devices.

■ CONCLUSION

Single ITO film and ITO/Au/ITO (IAI) sandwiched films were deposited on glass substrates via pulsed laser deposition. Structural, electrical, and optical properties of the samples were studied. Through ellipsometry measurements, the optical properties of each layer in the trilayer structure were successfully extracted. The result showed that the property of the Au spacer was highly dependent on its thickness. The optical and electrical properties of the upper ITO layer were improved by the insertion of the gold spacer. By manipulation of the thickness of the inserted gold layer, the plasma frequency of the sandwiched films was tuned accordingly, allowing the adjustment of the crossover frequency of the layered structure. Thus, this kind of configuration offers the potential as an alternative in plasmonic devices that operate in the NIR region.

■ ASSOCIATED CONTENT

ⓢ Supporting Information

Information on optical properties of Au in bulk and ultrathin layers; applicability and limitations of the effective medium approximation. This material is available free of charge via the Internet at http://pubs.acs.org.

■ AUTHOR INFORMATION

Corresponding Authors
*H.Y.: e-mail, huiye@zju.edu.cn; phone, (86)0571-87953979.
*C.W.L.: e-mail, dennis.leung@polyu.edu.hk; phone, (852) 2766 5670; fax, (852)23337629.

Notes
The authors declare no competing financial interest.

■ REFERENCES

(1) Barnes, W. L.; Dereux, A.; Ebbesen, T. W. Surface Plasmon Subwavelength Optics. *Nature* **2003**, *424* (6950), 824–830.

(2) Lal, S.; Link, S.; Halas, N. J. Nano-Optics from Sensing to Waveguiding. *Nat. Photonics* **2007**, *1* (11), 641–648.

(3) Smith, D. R.; Pendry, J. B.; Wiltshire, M. C. K. Metamaterials and Negative Refractive Index. *Science* **2004**, *305* (5685), 788–792.

(4) Tao, A. R. Metamaterials go Gattaca. *Nat. Photonics* **2014**, *8*, 6–8.

(5) Noginov, M. A.; Gu, L.; Livenere, J.; Zhu, G.; Pradhan, A. K.; Mundle, R.; Bahoura, M.; Barnakov, Yu. A.; Podolskiy, V. A. Transparent Conductive Oxides: Plasmonic Materials for Telecom Wavelengths. *Appl. Phys. Lett.* **2011**, *99* (2), 021101.

(6) Jablan, M.; Buljan, H.; Soljačić, M. Plasmonics in Graphene at Infrared Frequencies. *Phys. Rev. B* **2009**, *80* (24), 245435.

(7) Tassin, P.; Koschny, T.; Kafesaki, M.; Soukoulis, C. M. A Comparison of Graphene, Superconductors and Metals as Conductors for Metamaterials and Plasmonics. *Nat. Photonics* **2012**, *6* (4), 259–264.

(8) Alsaif, M. M. Y. A.; Latham, K.; Field, M. R.; Yao, D. D.; Medehkar, N. V.; Beane, G. A.; Kaner, R. B.; Russo, S. P.; Ou, J. Z.; Zalantar-zadeh, K. Tunable Plasmon Resonances in Two-Dimensional Molybdenum Oxide Nanoflakes. *Adv. Mater.* **2014**, *26*, 3931–3937.

(9) Naik, G. V.; Boltasseva, A. A Comparative Study of Semiconductor-Based Plasmonic Metamaterials. *Metamaterials* **2011**, *5*, 1–7.

(10) Naik, G. V.; Kim, J.; Boltasseva, A. Oxides and Nitrides as Alternative Plasmonic Materials in the Optical Range. *Opt. Mater. Exp.* **2011**, *1* (6), 1090–1099.

(11) Kim, J.; Naik, G. V.; Emani, N. K.; Boltasseva, A. Plasmonic Resonances in Nanostructured Transparent Conducting Oxide Films. **2012**, arXiv preprint arXiv:1211.5988.

(12) Naik, G. V.; Liu, J.; Kildishev, A. V.; Shalaev, V. M.; Boltasseva, A. Demonstration of Al: ZnO as a Plasmonic Component for Near-Infrared Metamaterials. *Proc. Natl. Acad. Sci. U.S.A.* **2012**, *109* (23), 8834–8838.

(13) Naik, G. V.; Shalaev, V. M.; Boltasseva, A. Alternative Plasmonic Materials: Beyond Gold and Silver. *Adv. Mater.* **2013**, *25* (24), 3264–3294.

(14) Cheng, X. R.; Hau, B. Y. H.; Endo, T.; Kerman, K. Au Nanoparticle-Modified DNA Sensor Based on Simultaneous Electrochemical Impedance Spectroscopy and Localized Surface Plasmon Resonance. *Biosens. Bioelectron.* **2014**, *53*, 513–518.

(15) Sharma, N. K.; Yadav, S.; Sajal, V. Theoretical Analysis of Highly Sensitive Prism Based Surface Plasmon Resonance Sensor with Indium Tin Oxide. *Opt. Commun.* **2014**, *318*, 74–78.

(16) Lounis, S. D.; Runnerstrom, E. L.; Bergerud, A.; Nordlund, D.; Milliron, D. J. Influence of Dopant Distribution on the Plasmonic Properties of Indium Tin Oxide Nanocrystals. *J. Am. Chem. Soc.* **2014**, *136*, 7110–7116.

(17) Li, S. Q.; Guo, P.; Buchholz, D. B. Plasmonic–Photonic Mode Coupling in Indium–Tin–Oxide Nanorod Arrays. *ACS Photonics* **2014**, *1* (3), 163–172.

(18) Clavero, C. Plasmon-Induced Hot-Electron Generation at Nanoparticle/Metal-Oxide Interfaces for Photovoltaic and Photocatalytic Devices. *Nat. Photonics* **2014**, *8* (2), 95–103.

(19) Roxworthy, B. J.; Bhuiya, A. M.; Vanka, S. P.; Toussaint, K. C., Jr. Understanding and Controlling Plasmon-Induced Convection. *Nat. Commun.* **2014**, *2*, 95–103.

(20) Michelotti, F.; Dominici, L.; Descrovi, E.; Danz, N.; Menchini, F. Thickness Dependence of Surface Plasmon Polariton Dispersion in Transparent Conducting Oxide Films at 1.55 μm. *Opt. Lett.* **2009**, *34* (6), 839–841.

(21) Rhodes, C.; Franzen, S.; Maria, J. P.; Losego, M.; Leonard, D. N.; Duscher, G.; Weibel, S. Surface Plasmon Resonance in Conducting Metal Oxides. *J. Appl. Phys.* **2006**, *100* (5), 054905-1-4.

(22) Losego, M. D.; Efremenko, A. Y.; Rhodes, C. L.; Cerruti, M. G.; Franzen, S.; Maria, J. P. Conductive Oxide Thin Films: Model Systems for Understanding and Controlling Surface Plasmon Resonance. *J. Appl. Phys.* **2009**, *106* (2), 024903-1-8.

(23) Rhodes, C.; Cerruti, M.; Efremenko, A.; Losego, M.; Aspnes, D. E.; Maria, J. P.; Franzen, S. Dependence of Plasmon Polaritons on the Thickness of Indium Tin Oxide Thin Films. *J. Appl. Phys.* **2008**, *103* (9), 093108-1-6.

(24) Franzen, S. Surface Plasmon Polaritons and Screened Plasma Absorption in Indium Tin Oxide Compared to Silver and Gold. *J. Phys. Chem. C* **2008**, *112* (15), 6027–6032.

(25) Guillén, C.; Herrero, J. TCO/Metal/TCO Structures for Energy and Flexible Electronics. *Thin Solid Films* **2011**, *520*, 1–17.

(26) Lee, J. H.; Woo, K. Y.; Kim, K. H.; Kim, H. D.; Kim, T. G. ITO/Ag/ITO Multilayer-Based Transparent Conductive Electrodes for Ultraviolet Light-Emitting Diodes. *Opt. Lett.* **2013**, *38* (23), 5055–5058.

(27) Girtan, M. Comparison of ITO/Metal/ITO and ZnO/Metal/ZnO Characteristics as Transparent Electrodes for Third Generation Solar Cells. *Sol. Energy Mater. Sol. Cells* **2012**, *100*, 153–161.

(28) Chakaroun, M.; Lucas, B.; Ratier, B.; Aldissi, M. ITO/Au/ITO Multilayer Electrodes for CuPc/C_{60} Solar Cells. *Energy Procedia* **2012**, *31*, 102–109.

(29) Kim, D. Low Temperature Deposition of Transparent Conducting ITO/Au/ITO Films by Reactive Magnetron Sputtering. *Appl. Surf. Sci.* **2010**, *256* (6), 1774–1777.

(30) Kim, Y. S.; Park, J. H.; Choi, D. H.; Jang, H. S.; Lee, J. H.; Park, J. I.; Ju, D. H.; Lee, J. Y.; Kim, D. ITO/Au/ITO Multilayer Thin Films for Transparent Conducting Electrode Applications. *Appl. Surf. Sci.* **2007**, *254* (5), 1524–1527.

(31) Yun, J.; Wang, W.; Bae, T. S.; Park, Y. H.; Kang, Y. C.; Kim, D. H.; Lee, S.; Lee, G. H.; Song, M.; Kang, J. W. Preparation of Flexible Organic Solar Cells with Highly Conductive and Transparent Metal-Oxide Multilayer Electrodes Based on Silver Oxide. *ACS Appl. Mater. Interfaces* **2013**, *5* (20), 9933–9941.

(32) Kim, D. The Influence of Au Thickness on the Structural, Optical and Electrical Properties of ZnO/Au/ZnO Multilayer Films. *Opt. Commun.* **2012**, *285* (6), 1212–1214.

(33) Philipp, M.; Knupfer, M.; Büchner, B.; Gerardin, H. Plasmonic Excitations in ZnO/Ag/ZnO Multilayer Systems: Insight into Interface and Bulk Electronic Properties. *J. Appl. Phys.* **2011**, *109* (6), 063710-1-6.

(34) Choi, K. H.; Choi, Y. Y.; Jeong, J. A.; Kim, H. K.; Jeon, S. Highly Transparent and Conductive Al-Doped ZnO/Ag/Al-Doped ZnO Multilayer Source/Drain Electrodes for Transparent Oxide Thin Film Transistors. *Electrochem. Solid-State Lett.* **2011**, *14* (4), 152–155.

(35) Cho, H. J.; Park, K. W.; Ahn, J. K. Nanoscale Silver Based Al Doped ZnO Multilayer Transparent Conductive Oxide Films. *J. Electrochem. Soc.* **2009**, *156*, 215–220.

(36) Park, H. K.; Kang, J. W.; Na, S. I.; Kim, D. Y.; Kim, H. K. Characteristics of Indium-Free GZO/Ag/GZO and AZO/Ag/AZO Multilayer Electrode Grown by Dual Target DC Sputtering at Room Temperature for Low-Cost Organic Photovoltaics. *Sol. Energy Mater. Sol. Cells* **2009**, *93* (11), 1994–2002.

(37) Dimopoulos, T.; Radnoczi, G. Z.; Pécz, B.; Brückl, H. Characterization of ZnO: Al/Au/ZnO: Al Trilayers for High

15751

dx.doi.org/10.1021/am5026165 | *ACS Appl. Mater. Interfaces* 2014, 6, 15743–15752

Performance Transparent Conducting Electrodes. *Thin Solid Films* **2010**, *519* (4), 1470−1474.

(38) Sytchkova, A.; Grilli, M. L.; Rinaldi, A.; Vedraine, S.; Torchio, P.; Piegari, A.; Flory, F. Radio Frequency Sputtered Al: ZnO-Ag Transparent Conductor: A Plasmonic Nanostructure with Enhanced Optical and Electrical Properties. *J. Appl. Phys.* **2013**, *114* (9), 094509-1-9.

(39) Guske, J. T.; Brown, J.; Welsh, A.; Franzen, S. Infrared Surface Plasmon Resonance of AZO-Ag-AZO Sandwich Thin Films. *Opt. Express* **2012**, *20* (21), 23215−23226.

(40) Kim, H.; Gilmore, C. M.; Horwitz, J. S.; Piqué, A.; Murata, H.; Kushto, G. P.; Schlaf, R.; Kafafi, Z. H.; Chrisey, D. B. Transparent Conducting Aluminum-Doped Zinc Oxide Thin Films for Organic Light Emitting Devices. *Appl. Phys. Lett.* **2000**, *76*, 259−261.

(41) Kim, H.; Horwitz, J. S.; Kim, W. H.; Makinen, A. J.; Kafafi, Z. H.; Chrisey, D. B. Doped ZnO Thin Films as Anode Materials for Organic Light-Emitting Diodes. *Thin Solid Films* **2002**, *420−421*, 539−543.

(42) Kim, S. H.; Park, N. M.; Kim, T. Y.; Yong, S. G. Electrical and Optical Characteristics of ITO Films by Pulsed Laser Deposition Using a 10 wt.% SnO_2-Doped In_2O_3 Ceramic Target. *Thin Solid Films* **2005**, *475*, 262−266.

(43) Minami, T. Present Status of Transparent Conducting Oxide Thin-Film Development for Indium-Tin-Oxide (ITO) Substitutes. *Thin Solid Films* **2008**, *516*, 5822−5828.

(44) Xin, J. Z.; Leung, C. W.; Chan, H. L. W. Composition Dependence of Structural and Optical Properties of $Ba(Zr_xTi_{1-x})O_3$ Thin Films Grown on MgO Substrates by Pulsed Laser Deposition. *Thin Solid Films* **2011**, *519* (19), 6313−6318.

(45) Sun, H.; Yu, M.; Wang, G.; Sun, X.; Lian, J. Temperature-Dependent Morphology Evolution and Surface Plasmon Absorption of Ultrathin Gold Island Films. *J. Phys. Chem. C* **2012**, *116* (16), 9000−9008.

(46) van der Pauw, L. J. A Method of Measuring Specific Resistivity and Hall Effect of Discs of Arbitrary Shape. *Philips Res. Rep.* **1958**, *13* (1), 1−9.

(47) Adurodija, F. O.; Izumi, H.; Ishihara, T.; Yoshioka, H.; Motoyama, M.; Murai, K. Pulsed Laser Deposition of Crystalline Indium Tin Oxide Films at Room Temperature by Substrate Laser Irradiation. *Jpn. J. Appl. Phys.* **2000**, *39* (4B), 377−379.

(48) Lee, S. W.; Joo, S. K. Low Temperature Poly-Si Thin-Film Transistor Fabrication by Metal-Induced Lateral Crystallization. *IEEE Electron Device Lett.* **1996**, *17* (4), 160−162.

(49) Stec, H. M.; Williams, R. J.; Jones, T. S.; Hatton, R. A. Ultrathin Transparent Au Electrodes for Organic Photovoltaics Fabricated Using a Mixed Mono-Molecular Nucleation Layer. *Adv. Funct. Mater.* **2011**, *21*, 1709−1716.

(50) Stoneham, A. M. Systematics of Metal-Insulator Interfacial Energies: A New Rule for Wetting and Strong Catalyst-Support Interactions. *Appl. Surf. Sci.* **1983**, *14* (3), 249−259.

(51) Didier, F.; Jupille, J. Simple Views on Metal/Oxide Interfaces: Contributions of the Long-Range Interactions to the Adhesion Energy. *J. Adhes.* **1996**, *58* (3−4), 253−261.

(52) Szunerits, S.; Praig, V. G.; Manesse, M.; Boukherroub, R. Gold Island Films on Indium Tin Oxide for Localized Surface Plasmon Sensing. *Nanotechnology* **2008**, *19* (19), 195712-1-7.

(53) Sun, X. W.; Huang, H. C.; Kwok, H. S. On the initial growth of indium tin oxide on glass. *J. Appl. Phys.* **1996**, *68* (19), 2663−2665.

(54) Leung, C. W.; Vickers, M. E.; Buchanan, J. D. R.; Blamire, M. G. A Study of Conventional Top Spin Valve Structure through the Built-Up Samples Technique. *J. Magn. Magn. Mater.* **2004**, *269* (1), 15−29.

(55) Lowndes, D. H.; Geohegan, D. B.; Puretzky, A. A.; Norton, D. P.; Rouleau, C. M. Synthesis of Novel Thin-Film Materials by Pulsed Laser. *Science* **1996**, *273*, 898−903.

(56) Kim, H.; Gilmore, C. M.; Pique, A.; Horwitz, J. S.; Mattoussi, H.; Murata, H.; Kafafi, Z. H.; Chrisey, D. B. Electrical, Optical, and Structural Properties of Indium−Tin−Oxide Thin Films for Organic Light-Emitting Devices. *J. Appl. Phys.* **1999**, *86* (11), 6451−6461.

(57) Choi, Y. Y.; Choi, K. H.; Lee, H..; Lee, H.; Kang, J. W.; Kim, H. K. Nano-Sized Ag-Inserted Amorphous $ZnSnO_3$ Multilayer Electrodes for Cost-Efficient Inverted Organic Solar Cells. *Sol. Energy Mater. Sol. Cells.* **2011**, *95* (7), 1615−1623.

(58) Jeong, J. A.; Park, Y. S.; Kim, H. K. Comparison of Electrical, Optical, Structural, and Interface Properties of IZO-Ag-IZO and IZO-Au-IZO Multilayer Electrodes for Organic Photovoltaics. *J. Appl. Phys.* **2010**, *107* (2), 023111-1-8.

(59) Bender, M.; Seelig, W.; Daube, C.; Frankenberger, H.; Ocker, B.; Stollenwerk, J. Dependence of Film Composition and Thicknesses on Optical and Electrical Properties of ITO−Metal−ITO Multilayers. *Thin Solid Films* **1998**, *326*, 67−71.

(60) Feigenbaum, E.; Diest, K.; Atwater, H. A. Unity-Order Index Change in Transparent Conducting Oxides at Visible Frequencies. *Nano Lett.* **2010**, *10* (6), 2111−2116.

(61) Wang, K. K.; Hua, Y. F.; Wang, J.; Song, C. L.; Jia, S. H.; Han, G. R.; Liu, Y. Optical and Structural Characterization of SnO_2:F/SiC_xO_y Tandem Thin Films by Spectroscopic Ellipsometry. *Thin Solid Films* **2013**, *540*, 84−91.

(62) Henriquez, R.; Flores, M.; Moraga, L.; Kremer, G.; Fuentesa, C. G.; Munozb, R. C. Electron Scattering at Surfaces and Grain Boundaries in Thin Au Films. *Appl. Surf. Sci.* **2013**, *273*, 315−323.

(63) Ma, W. G.; Wang, H. D.; Zhang, X.; Wang, W. Experiment Study of the Size Effects on Electron−Phonon Relaxation and Electrical Resistivity of Polycrystalline Thin Gold Films. *J. Appl. Phys.* **2010**, *108*, 064308-1-7.

(64) Jennings, T.; Strouse, G. Past, Present, and Future of Gold Nanoparticles. *Bio-Applications of Nanoparticles*; Chen, W. C. W., Ed.; Springer: New York, 2007; Chapter 3, pp 34−46; http://link.springer.com/chapter/10.1007/978-0-387-76713-0_3 (accessed August 16, 2014).

(65) Agranovich, V. M.; Kravtsov, V. E. Notes on Crystal Optics of Superlattices. *Solid State Commun.* **1985**, *55* (1), 85−90.

(66) Poddubny, A.; Iorsh, I.; Belov, P.; Kivshar, Y. Hyperbolic Metamaterials. *Nat. Photonics* **2013**, *7*, 958−967.

(67) Kim, J.; Drachev, V. P.; Jacob, Z.; Naik, G. V.; Boltasseva, A.; Narimanov, E. E.; Shalaev, V. M. Improving the Radiative Decay Rate for Dye Molecules with Hyperbolic Metamaterials. *Opt. Express* **2012**, *20* (7), 8100−8116.

(68) Korobkin, D.; Neuner, B.; Fetz, C.; Jegenyes, N.; Ferro, G.; Shvets, G. Measurements of the Negative Refractive Index of Sub-Diffraction Waves Propagating in an Indefinite Permittivity Medium. *Opt. Express* **2010**, *18* (22), 22734−22746.

(69) West, P. R.; Ishii, S.; Naik, G. V.; Emani, N. K.; Shalaev, V. M.; Boltasseva, A. Searching for Better Plasmonic Materials. *Laser Photonics Rev.* **2010**, *4* (6), 795−808.

(70) Szunerits, S.; Castel, X.; Boukherroub, R. Surface Plasmon Resonance Investigation of Silver and Gold Films Coated with Thin Indium Tin Oxide Layers: Influence on Stability and Sensitivity. *J. Phys. Chem. C* **2008**, *112*, 15813−15817.